Assesment of Single-Dipole and Dual-Dipole Inverse Solutions in Electrocardiography

V. Jazbinsek[1] and R. Hren[1]

[1] Institute of Mathematics, Physics and Mechanics, Jadranska 19, Ljubljana, Slovenia

Abstract— **In this study, we closely examined the performance of a well-known inverse solution in terms of equivalent dipole source model. To simulate potential distribution on the "body surface", we employed an analytical model of a single current dipole (or a pair of current dipoles) placed within the homogeneous isotropic volume conductor consisting of two non-concentric spheres. Using these data, we evaluated the accuracy of recovering both location and orientation of the single or dual dipole sources. In total, we examined 24 different dipole locations and found that the location of both fitted single current dipoles and dual current dipoles virtually coincided with the original source for high S/N ratios. While our results corroborate findings obtained with more complex geometry, our tool provides an efficient and analytical means in assessing electrocardiographic inverse solutions.**

Keywords— **electrocardiography, inverse problem, current dipole**

I. Introduction

Mathematical modeling of both source and volume conductor remains one of the prerequisites for any quantitative interpretation of electrocardiographic data. One of the rather simple models employs a single dipole source model within the homogeneous and isotropic torso model to represent the cardiac current generator and electric properties of the human body, respectively. Several studies have investigated how, for example, the torso inhomogeneity or the individualization of the human torsos may affect the accuracy of an inverse solution [1]. Here, we have chosen rather different - "back-to-basics" approach - where our intention is to create the analytical model which may serve as an efficient tool in examining performance of electrocardiographic inverse solution in terms of models, which use either single current dipoles or dual current dipoles.

II. Methods

To model the "thoracic" volume conductor, we used a pair of homogeneous and isotropic non-concentric spheres and placed either a single current dipole or a pair of two dipoles inside of the smaller sphere. When using such an obviously simplified model, the potentials at an arbitrary point can be calculated analytically in the closed form [2], however, as it can be clearly seen from the Appendix, even such a compact form possesses some computational challenges.

We approximated the body surface by the homogeneous conducting sphere with the unity radius ($R_{\mathrm{B}} = 1$), and the epicardial surface by a smaller sphere with a radius of $R_{\mathrm{E}} = 0.5$, positioned eccentrically $\vec{r}_{\mathrm{E}} = (0.1, -0.2, 0.3)$. The body and the epicardial surfaces were tessellated using 1280 and 720 triangles (642 and 362 nodes), respectively. The tessellation of the body surfaces was generated by refinement of icosahedron in four steps and the epicardial surface was generated by refinement of truncated icosahedron in two steps. In this paper, we tested three electrode systems, each having 32 leads, see Fig. 1.

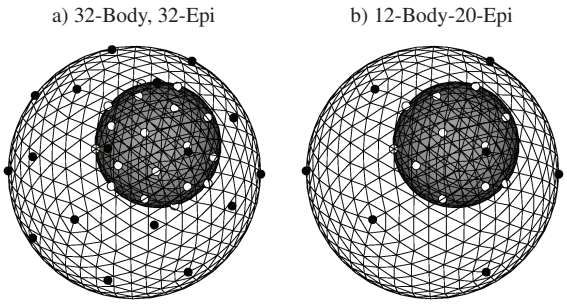

Fig. 1: Lead systems used in the fitting procedure: a) 32-leads on the body and 32-leads on the epicardium, and b) combination of 12-leads on the body and 20-leads on the epicardium. Leads on the body (outer sphere) are denoted with •, leads on the epicardium(inner sphere) are denoted with ○.

We put the single dipole source model in the total of 24 locations, 12 in nodes of icosahedron positioned near the center of the body surface and 12 in nodes of icosahedron positioned near the center of the epicardial surface. Both source icosahedrons have same dimension defined by circumsribed sphere radius of 0.3. In each of the positions, we put 3 single current dipoles pointing along axes of the Cartesian coordinate system, which gives total of 72 single dipole sources.

For the dual dipole model, we combined node positions of both source icosahedrons to construct 12 most close posi-

Á. Jobbágy (Ed.): 5th European IFMBE Conference, IFMBE Proceedings 37, pp. 323–326, 2011.
www.springerlink.com

tioned pairs (mean distance 0.178 ± 0.069), 12 most distant positioned pairs (mean distance 0.696 ± 0.026), and 12 pairs of corresponding nodes shifted by $\vec{r}_{\mathrm{E}}$ (median, $||\vec{r}_{\mathrm{E}}|| = 0.374$). In each of the pairs, we put either 3 parallel or anti-parallel or perpendicular dipoles pointing along axes of the Cartesian coordinate system. For each type of distance (close, median, distant) and each type of direction (parallel, anti-parallel, perpendicular), we therefore obtain 36 dual dipole sources.

For all single and dual dipole sources, we calculated potential maps on three lead systems from Fig. 1 using analytical solution described in the Appendix. In order to test the inverse solution, we added to the analytically calculated maps 7 different noise levels (*S/N*=10,15,...,40 dB), where

$$S/N = 20\log_{10}\frac{\mathrm{RMS(signal)}}{\mathrm{RMS(noise)}}\,. \qquad (1)$$

For each analytically calculated map and for each noise level, we generated 10 different random noise distributions and performed the inverse solutions either for a single-dipole model or dual-dipoles model.

As a measure of localization accuracy, we used the distance between the recovered location(s) and original location(s) of dipole(s). In addition, we also calculated relative errors between noisy ($\mathbf{V}_{\mathrm{n}}$) and fitted ($\mathbf{V}_{\mathrm{f}}$) maps ($\mathrm{RE_{fn}}$), and between analytical ($\mathbf{V}_{\mathrm{a}}$) and fitted maps ($\mathrm{RE_{fn}}$):

$$\mathrm{RE_{fn}} = \frac{||\mathbf{V}_{\mathrm{f}} - \mathbf{V}_{\mathrm{n}}||_2}{||\mathbf{V}_{\mathrm{n}}||_2}\,,\ \mathrm{RE_{fa}} = \frac{||\mathbf{V}_{\mathrm{f}} - \mathbf{V}_{\mathrm{a}}||_2}{||\mathbf{V}_{\mathrm{a}}||_2}\,. \qquad (2)$$

III. Results

Table 1 and Fig. 2 display average single dipole source localization errors (Δr) and REs calculated with different lead system and noise levels, where

$$\Delta r = ||\vec{r}_f - \vec{r}_p||_2\,, \qquad (3)$$

and $\vec{r}_f$ and $\vec{r}_p$ are fitted and original dipole locations, respectively. Results clearly show that for high *S/N* ratio (40 dB) location of the single current dipole almost coincide with the original source for all lead systems. The 32-Epi lead system outperforms the other two in terms of localization error. On the other hand, relative fit errors $\mathrm{RE_{fn}}$ are almost the same for all lead systems. Note, that fitted potential maps are more similar to the analytical maps than noisy maps ($\mathrm{RE_{fa}} < \mathrm{RE_{fn}}$).

Fig. 3 displays Δr and REs in logarithmic scale. We observe linear dependence of both $\log(\Delta r/R)$ and $\log(\mathrm{RE})$ vs. *S/N*. According to Eq. (1), both Δr and RE are therefore proportional to noise RMS value.

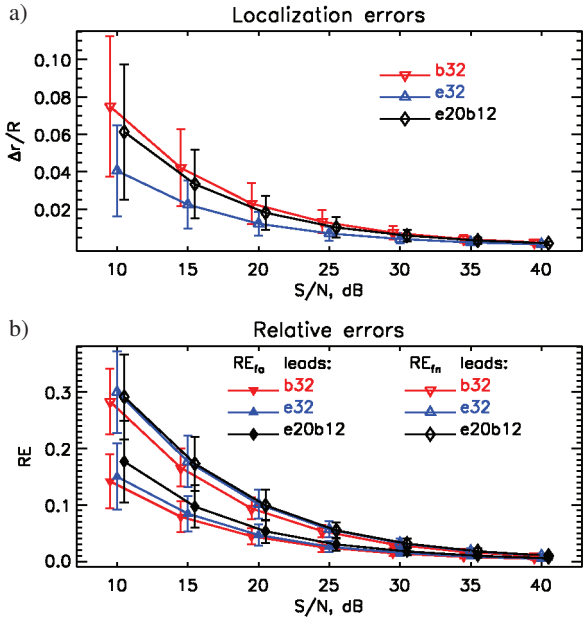

Fig. 2: a) Localization errors ($\Delta r/R$) and b) relative errors ($\mathrm{RE_{fn}}$ and $\mathrm{RE_{fa}}$) vs. noise levels for single dipole sources.

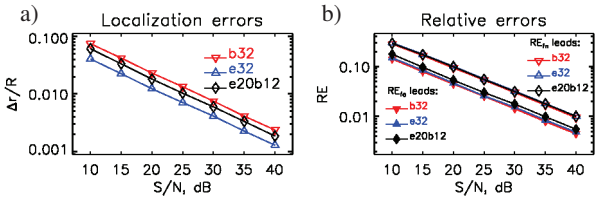

Fig. 3: Logarithmic scaling of a) localization errors and b) relative errors for single dipole sources.

Table 2 displays average dual dipole source localization errors (Δr_1, Δr_2 and Δr_{c}) and REs calculated by 32-Epi lead system using data with different noise levels generated with dual dipole sources with different mutual distances and orientations. Localization errors are defined as distances between the recovered locations ($\vec{r}_{f1}$, $\vec{r}_{f2}$) and original locations ($\vec{r}_{p1}$, $\vec{r}_{p2}$) of both dipoles. Combined error is defined as

$$\Delta r_{\mathrm{c}} = \sqrt{\Delta r_1^2 + \Delta r_2^2}\,, \qquad (4)$$

and it is shown in Fig. 4. Results show that distance between dipoles in the dual dipole source model plays an important role in the source localization procedure. In the presence of noise, locations of close positioned dipoles are poorly recovered. On the other hand, mutual orientation between dipoles is not so important.

Table 1: Single dipole fit results averaged over 720 samples (72 single dipole sources × 10 random noise distributions) for different lead systems and noise levels.

Noise	32-Body			32-Epi			12-Body-20-Epi		
[dB]	$\Delta r/R$±SD	RE_{fn}±SD	RE_{fa}±SD	$\Delta r/R$±SD	RE_{fn}±SD	RE_{fa}±SD	$\Delta r/R$±SD	RE_{fn}±SD	RE_{fa}±SD
10	0.075±0.037	0.283±0.058	0.142±0.048	0.041±0.024	0.300±0.072	0.150±0.059	0.061±0.036	0.291±0.075	0.177±0.073
20	0.023±0.011	0.094±0.019	0.045±0.014	0.012±0.006	0.101±0.026	0.047±0.019	0.018±0.009	0.099±0.027	0.053±0.021
30	0.007±0.004	0.030±0.006	0.014±0.005	0.004±0.002	0.032±0.008	0.015±0.006	0.006±0.003	0.031±0.008	0.018±0.007
40	0.002±0.001	0.009±0.002	0.004±0.002	0.001±0.001	0.010±0.003	0.005±0.002	0.002±0.001	0.010±0.003	0.006±0.002

Table 2: Dual dipole fit results using 32-Epi lead system averaged over 360 samples (36 dual dipole sources × 10 random noise distributions) for different *S/N* and groups of distances and orientations between two single dipoles that forming dual dipole sources.

	S/N	Parallel dipoles					Anti-parallel dipoles					Perpendicular dipoles				
	[dB]	$\Delta r_1/R$	$\Delta r_2/R$	$\Delta r_c/R$±SD	RE_{fn}	RE_{fa}	$\Delta r_1/R$	$\Delta r_2/R$	$\Delta r_c/R$±SD	RE_{fn}	RE_{fa}	$\Delta r_1/R$	$\Delta r_2/R$	$\Delta r_c/R$±SD	RE_{fn}	RE_{fa}
close	10	0.163	0.162	0.262±0.123	0.223	0.206	0.197	0.204	0.291±0.163	0.590	1.389	0.160	0.161	0.247±0.115	0.300	0.293
	20	0.093	0.088	0.148±0.116	0.077	0.063	0.081	0.080	0.117±0.114	0.346	0.409	0.063	0.060	0.096±0.083	0.108	0.086
	30	0.033	0.031	0.051±0.077	0.025	0.020	0.029	0.029	0.042±0.047	0.149	0.128	0.022	0.021	0.033±0.034	0.034	0.027
	40	0.013	0.013	0.021±0.058	0.008	0.006	0.009	0.008	0.012±0.013	0.050	0.038	0.007	0.007	0.010±0.010	0.011	0.008
median	10	0.116	0.101	0.166±0.086	0.199	0.177	0.122	0.086	0.156±0.074	0.363	0.345	0.117	0.086	0.152±0.068	0.249	0.229
	20	0.033	0.031	0.048±0.026	0.068	0.054	0.030	0.030	0.045±0.022	0.134	0.106	0.030	0.026	0.042±0.018	0.088	0.067
	30	0.010	0.013	0.018±0.019	0.022	0.017	0.010	0.010	0.015±0.009	0.043	0.032	0.009	0.008	0.013±0.009	0.028	0.021
	40	0.003	0.003	0.005±0.003	0.007	0.005	0.003	0.003	0.005±0.004	0.013	0.011	0.003	0.003	0.004±0.002	0.008	0.007
distant	10	0.061	0.068	0.097±0.044	0.183	0.148	0.051	0.059	0.083±0.037	0.224	0.183	0.055	0.059	0.086±0.039	0.199	0.160
	20	0.018	0.021	0.029±0.018	0.059	0.047	0.017	0.021	0.029±0.019	0.075	0.057	0.018	0.021	0.030±0.018	0.065	0.051
	30	0.006	0.006	0.009±0.005	0.019	0.015	0.005	0.006	0.009±0.005	0.024	0.018	0.005	0.006	0.008±0.004	0.021	0.016
	40	0.002	0.002	0.003±0.001	0.006	0.005	0.002	0.002	0.003±0.001	0.007	0.006	0.002	0.002	0.003±0.001	0.007	0.005

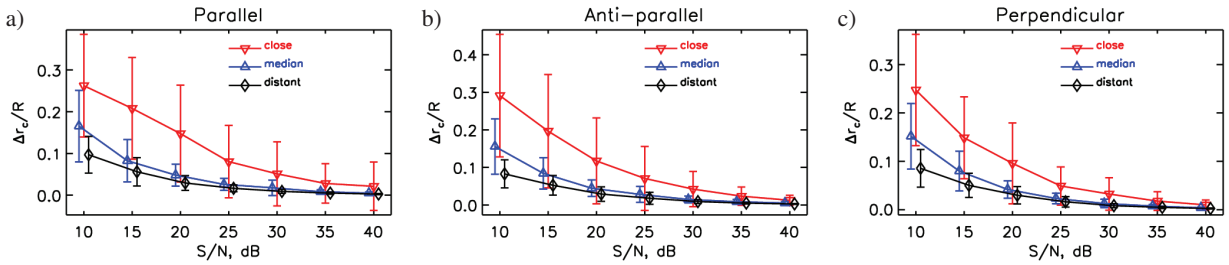

Fig. 4: Localization errors ($\Delta r_c/R$) calculated with 32-epi lead system for dual dipole sources with a) parallel, b) anti-parallel and c) perpedicular mutual directions and different distances between dipoles that forming dual sources.

IV. Conclusions

In this simulation, we constructed a simplified analytically solvable source and volume conductor model for evaluation electrocardiographic inverse problem solutions. Main findings are

- lead systems positioned closer to sources are more efficient
- both fitted single current dipoles and dual current dipoles virtually coincided with the original source for high S/N ratios
- dual current dipole location recovery is sensitive to the distance between the original dipoles.

A Appendix: Analytical Solution

Electric potential on a surface and within a conducting sphere with radius R generated by an arbitrary dipole $\vec{p}$ at location $\vec{r}_p$ anywhere ($\vec{r} \neq \vec{r}_p$) within the sphere can be solved analytically by a closed solution derived by Yao[2]

$$V(\vec{r}) = \frac{\vec{p}}{4\pi\sigma R^3} \cdot \left\{ \frac{R^3(\vec{r}-\vec{r}_p)}{|\vec{r}-\vec{r}_p|^3} + \frac{1}{r_{pi}^3}\left(\vec{r} - \frac{r^2}{R^2}\vec{r}_p\right) + \frac{1}{r_{pi}}\left[\vec{r} + \frac{(\vec{r}\cdot\vec{r}_p)\vec{r} - r^2\vec{r}_p}{R^2(r_{pi}+1) - (\vec{r}\cdot\vec{r}_p)}\right]\right\}, \quad (5)$$

where $r = |\vec{r}|$, $r_p = |\vec{r}_p|$ and

$$r_{pi} = \left[1 + \left(\frac{r_p r}{R^2}\right)^2 - 2\frac{(\vec{r}\cdot\vec{r}_p)}{R^2}\right]^{1/2}. \quad (6)$$

Note, that in the original formula (Eq. (13) in [2]), the $(\vec{r}\cdot\vec{r}_p)$ is expressed as $(r_p r\cos\varphi)$, where φ is the angle between $\vec{r}$ and $\vec{r}_p$. For the surface potential, $r\equiv R$, $Rr_{pi}=|\vec{R}-\vec{r}_p|$, Eq. (1) is simplified to

$$V(\vec{R}) = \frac{\vec{p}}{4\pi\sigma R^3}\cdot\left\{2\frac{R^3(\vec{R}-\vec{r}_p)}{|\vec{R}-\vec{r}_p|^3} + \frac{R}{|\vec{R}-\vec{r}_p|}\left[\vec{R}+\frac{(\vec{R}\cdot\vec{r}_p)\vec{R}-R\vec{r}_p}{|\vec{R}-\vec{r}_p|+R-r_p\cos\varphi}\right]\right\}, \quad (7)$$

which is the same as the formula derived by Brody et al. [3]. For a special case, when the current dipole is in the center of the conducting sphere ($r_p=0$), we get well known result $V(\vec{R})=3\frac{\vec{p}\cdot\vec{R}}{4\pi\sigma R^3}=3V_\infty(\vec{R})$, where V_∞ is the potential generated by the current dipole source in an infinite conducting space.

The general solution (5) can be re-arranged in the following form, which is more suitable for applying it in computer programmes and calculating derivatives

$$V(\vec{r})=\frac{1}{4\pi\sigma R^3}\left[f(\vec{r})(\vec{p}\cdot\vec{r})-g(\vec{r})(\vec{p}\cdot\vec{r}_p)\right], \quad (8)$$

where

$$f(\vec{r}) = \frac{R^3}{|\vec{r}-\vec{r}_p|^3}+\frac{1}{r_{pi}}\left[1+\frac{1}{r_{pi}^2}+\frac{(\vec{r}\cdot\vec{r}_p)}{R^2(r_{pi}+1)-(\vec{r}\cdot\vec{r}_p)}\right] = f_1(\vec{r})+\frac{1+f_2(\vec{r})+f_3(\vec{r})}{r_{pi}}, \quad (9)$$

and

$$g(\vec{r}) = \frac{R^3}{|\vec{r}-\vec{r}_p|^3}+\frac{1}{r_{pi}}\left[\frac{1}{r_{pi}^2}\frac{r^2}{R^2}+\frac{r^2}{R^2(r_{pi}+1)-(\vec{r}\cdot\vec{r}_p)}\right] = g_1(\vec{r})+\frac{g_2(\vec{r})+g_3(\vec{r})}{r_{pi}}, \quad (10)$$

where $f_1(\vec{r})=g_1(\vec{r})=\frac{R^3}{|\vec{r}-\vec{r}_p|^3}$, $f_2(\vec{r})=\frac{1}{r_{pi}^2}$, $f_3(\vec{r})=\frac{\vec{r}\cdot\vec{r}_p}{D}$,
$g_2(\vec{r})=\frac{r^2}{R^2}f_2(\vec{r})$, $g_3(\vec{r})=\frac{r^2}{D}$, and $D=R^2(r_{pi}+1)-\vec{r}\cdot\vec{r}_p$.

During nonlinear least square fitting procedures, when we are looking for the optimal source parameters, i.e. dipole location $\vec{r}_p$ and dipole strength $\vec{p}$, we need also partial derivatives over those parameters that can be expressed as

$$\nabla_p V=\left(\frac{\partial V}{\partial x_p},\frac{\partial V}{\partial y_p},\frac{\partial V}{\partial z_p}\right) \text{ and } \nabla_s V=\left(\frac{\partial V}{\partial p_x},\frac{\partial V}{\partial p_y},\frac{\partial V}{\partial p_z}\right), \quad (11)$$

where ∇_p and ∇_s represent gradients of source location and source strength, respectively. Gradient of potential (8) can be generally expressed as

$$\nabla V(\vec{r}) = \frac{1}{4\pi\sigma R^3}\Big[f(\vec{r})\nabla(\vec{p}\cdot\vec{r})+(\vec{p}\cdot\vec{r})\nabla f(\vec{r}) - f(\vec{r})\nabla(\vec{p}\cdot\vec{r}_p)-(\vec{p}\cdot\vec{r}_p)\nabla g(\vec{r})\Big]. \quad (12)$$

Components of source strength are included only in $(\vec{p}\cdot\vec{r})$ and $(\vec{p}\cdot\vec{r}_p)$, what leads to

$$\nabla_s V(\vec{r})=\frac{1}{4\pi\sigma R^3}\left[f(\vec{r})\,\vec{r}-g(\vec{r})\,\vec{r}_p\right], \quad (13)$$

and the potential in (8) can be written as

$$V(\vec{r})=\vec{p}\cdot\nabla_s V(\vec{r}). \quad (14)$$

The above formula can be used in linear least square fitting procedures [4], where the source location is known and only the source sthregth has to be determined.

On the other hand, components of source coordinates $\vec{r}_p$ are also included in $f(\vec{r})$, $g(\vec{r})$ and r_{pi}. Consequently, non-linear least square, like the Levengerg-Marquardt algoritm [4], has to be applied in the fitting procedure. From (8) and (12) it follows

$$\nabla_p V=\frac{1}{4\pi\sigma R^3}\left[(\vec{p}\cdot\vec{r})\nabla_p f-g\,\vec{p}-(\vec{p}\cdot\vec{r}_p)\nabla_p g\right), \quad (15)$$

where $\nabla_p f$ and $\nabla_p g$ are

$$\nabla_p f=\nabla f_1+\frac{\nabla f_2+\nabla f_3}{r_{pi}}-\frac{\nabla r_{pi}}{r_{pi}^2}\left(1+f_2+f_3\right) \quad (16)$$

$$\nabla_p g=\nabla g_1+\frac{\nabla g_2+\nabla g_3}{r_{pi}}-\frac{\nabla r_{pi}}{r_{pi}^2}\left(g_2+g_3\right), \quad (17)$$

where $\nabla_p f_1=\nabla_p g_1=3R^3\frac{\vec{r}-\vec{r}_p}{|\vec{r}-\vec{r}_p|^5}$, $\nabla_p f_2=-2\frac{\nabla_p r_{pi}}{r_{pi}^3}$,

$\nabla_p f_3=\frac{\vec{r}}{D}-(\vec{r}\cdot\vec{r}_p)\frac{\nabla_p D}{D^2}$, $\nabla_p g_2=\frac{r^2}{R^2}\nabla_p f_2$, $\nabla_p g_3=-r^2\frac{\nabla_p D}{D^2}$,

$\nabla_p r_{pi}=\frac{1}{R^2 r_{pi}}\left[\frac{r^2}{R^2}\vec{r}-\vec{r}\right]$, $\nabla_p D=R^2\nabla_p r_{pi}-\vec{r}_p$.

REFERENCES

1. Hren R, Stroink G, Horáček BM (1998) Accuracy of single-dipole inverse solution when localising ventricular pre-excitation sites: simulation study. Med Biol Eng Comp 36:323–329
2. Yao D (2000) Electric Potential Produced by a Dipole in a Homogeneous Conducting Sphere. IEEE Trans Biomed Eng BME-44:964-966
3. Brody DA, Terry FH, Ideker RE (1973) Eccentric dipole in a spherical medium: generalized expression for surface potentials. IEEE Trans Biomed Eng BME-20:141–143
4. Press WH, Flannery BP, Teukolsky SA, Vetterling WT (1989) Numerical Recipes - The Art of Scientific Computing, Cambridge University Press

Author: Vojko Jazbinšek
Institute: Institute of Mathematics, Physics and Mechanics
Street: Jadranska 19
City: SI-1000 Ljubljana
Country: Slovenija
Email: vojko.jazbinsek@imfm.si